의학 박사 학위논문

고에너지 방사선에 의한 심근의 구조적 기능적 변화에 관한 연구

–부정맥 치료를 위한 비침습적 심장 방사선 치료 기전에 관한 고찰–

2021 년 2 월

서울대학교 대학원

의학과 의학전공

차 명 진

고에너지 방사선에 의한
심근의 구조적 기능적 변화에 관한 연구

–부정맥 치료를 위한 비침습적 심장 방사선 치료 기전에 관한 고찰–

지도 교수 오 세 일

이 논문을 의학박사 학위논문으로 제출함
2020 년 10 월

서울대학교 대학원
의학과 의학전공
차 명 진

차명진의 의학박사 학위논문을 인준함
2021 년 1 월

위 원 장 서 정 욱 (인)
부위원장 은 시 아 (인)
위 원 강 경 환 (인)
위 원 김 병 아 (인)
위 원 최 기 준 (인)

초 록

Myocardial structural and functional changes by high-dose irradiation : implication for noninvasive cardiac radioablation for cardiac arrhythmias

Myung-Jin Cha
Medicine Major
Dept. of Medicine
The Graduate School
Seoul National University

Noninvasive radioablation, termed stereotactic body radiotherapy or stereotactic ablative radiation therapy in the radiation oncology field, was recently introduced as an alternative noninvasive treatment modality for fatal ventricular tachycardia (VT). However, myocardial changes leading to early-period antiarrhythmic effects induced by high-dose irradiation are unknown. The presumed mechanism of antiarrhythmic effect of radioablation was fibrosis, which occurs several months after irradiation and proof of principle studies on pulmonary vein isolation demonstrated effective conduction block with radiation-induced fibrosis. In the previous human clinical study, antiarrhythmic effects after radioablation commence at various time points, ranging from immediately post-radioablation to 6 months post-treatment.

In the current ongoing human clinical trial, I also observed the burden of the VT, whereby it decreased within a period of two weeks in all five study patients. The VT cycle length, the QRS morphology, and coupling interval of VT were changed.

To reveal the pathologic mechanism of this early antiarrhythmic effect of high-dose irradiation, I investigated dose-responsive histologic, ultrastructural, and functional changes within 1 month after irradiation in rat heart. Whole hearts of wild-type Lewis rats (N = 95) were irradiated with single fraction 20, 25, 30, 40, or 50 Gy and explanted at 1 day or 1, 2, 3, or 4 weeks post-irradiation. Microscopic pathologic changes of cardiac structures by light microscope with immunohistopathologic staining, ultrastructure by

electron microscopy, and functional evaluation by electrocardiography (ECG) and echocardiography were studied. Despite high dose irradiation, no myocardial necrosis or apoptosis was observed. Intercalated discs were widened and disrupted, forming uneven and twisted junctions between adjacent myocytes. Diffuse vacuolization peaked at 3 weeks, suggesting irradiation dose-responsiveness, which was correlated with interstitial and intracellular edema. CD68 immunostaining accompanying vacuolization suggested mononuclear cell infiltration. These changes were prominent in working myocardium but not cardiac conduction tissue. Intracardiac conduction represented by PR and QTc intervals on ECG was delayed compared to baseline measurements. ST segment depressed till 1 week, but elevated after 2 weeks. Ventricular chamber dimensions and function remained intact without pericardial effusion.

In summary, I observed a significant decrease in VT burden within a few days in five cardiac radioablation patients. In in-vivo study using rat model, mononuclear cell-related intra- and extracellular edema with diffuse vacuolization and intercalated disc widening were observed within 2 weeks after high-dose irradiation. ECG indicated intracardiac conduction delay with prominent ST-segment changes. These observations suggest that early antiarrhythmic effects after cardiac radioablation result from conduction disturbances and membrane potential alterations without necrosis.

.....

Keywords: cardiac radioablation, ventricular tachycardia, radiofrequency ablation, radiotherapy, myocardium, ultrastructure

Student Number: 2013-30602

목 차

Tables

Figures

Chapter 1. Introduction

1.1. Study Background

Noninvasive radioablation delivered with stereotactic body radiotherapy (SBRT) or stereotactic ablative radiation (SABR) therapy in the radiation oncology field, was recently introduced as an alternative noninvasive treatment modality for fatal ventricular arrhythmia.(1, 2) Patients with ventricular tachycardia (VT) can be treated with antiarrhythmic drugs or invasive catheter ablation procedures to reduce VT recurrences. However, conventional treatment failure is not unusual and recurrence remains an import clinical issue.

The radiofrequency catheter ablation procedure which is the standard therapy for VT identify the VT focus and then deliver thermal energy to the VT target lesion such as myocardial scar. Although there were continued advances in ablation techniques, catheter ablation may be ineffective for lots of patients.(3) Failure is most commonly caused by an inability to accurately identify the VT substrate, extensive substrate not amenable to effective ablation, or substrate inaccessible with current technologies.(4) There is need to develop the alternative therapies for treating VT.

In 2017, Dr. Cuculich and Dr. Robinson with their colleagues reported a marked reduction in the burden of VT was achieved with a noninvasive method for mapping and treating the arrhythmogenic focus of the heart in the refractory VT cases.(5) Currently, this noninvasive cardiac radioablation experience in human is still limited but steadily growing since the first reported cases in 2014.(6, 7) The global cases or clinical trials show a promising the efficacy and safety data of cardiac radioablation.(8) Therefore further research regarding the mechanism of action is important to making this novel therapy a success.(8)

The exact mechanism of antiarrhythmic effect of cardiac radioablation is not yet known well. The presumed mechanism of antiarrhythmic effect of radioablation was tissue fibrosis, which occurs several months after irradiation and proof of principle studies on pulmonary vein isolation demonstrated effective conduction block with radiation-induced fibrosis.(9, 10) However, antiarrhythmic effects after radioablation commence at various time points, ranging from immediately post-radioablation to 6 months post-treatment.(1, 2, 11, 12) Compared to late response, the cause of early antiarrhythmic effects from radioablation remains unknown, as most studies have focused on fibrosis after radioablation in soft tissues. Another explanation of antiarrhythmic effect of irradiation

is the upregulation of the gap junction protein connexin-43.(8) This upregulation was observed after 2 weeks and lasted for over 1 year.(13-15)

The VT is associated with an increased risk of sudden death,(16) which needs urgent treatment. Therefore, physicians usually expect the acute or early response of VT treatment. However, acute or early period effects on heart in the aspect of tissue response of cardiac radioablation are not yet studied well. Pioneering studies in the 1970s to 1980s investigated radiation induced pathologic effects on the heart (17-20), focusing on cardiac toxicity after radiation therapy. Nevertheless, current clinical needs require the assessment of high-dose irradiation effects at a cellular level at early time points to understand the early antiarrhythmic mechanisms of radiation.

1.2. Purpose of Research

In this study, I described early antiarrhythmic response in my clinical experiences on the human cardiac radioablation cases. To investigate the mechanism of this early response of irradiation, the animal study using rat model focused on early-period high-dose irradiation effects within 1 month on myocardial components in the *in vivo* study. Altogether, by observing clinical response in

human and structural changes in the rat heart after irradiation, I expect to understand the mechanism of antiarrhythmic effect that appears early after cardiac radioablation.

Chapter 2. Noninvasive Cardiac Radioablation for Ventricular Tachycardia

2.1. Methods

2.1.1. Clinical study design

The HeartSABR trial (arrhythmias treatment in Heart using Stereotactic ABlative Radiation therapy) is an ongoing prospective single-arm phase I/II trial conducted at a single center. The patient's informed consent for radiotherapy under clinical trial (HeartSABR, KCT0004302) was obtained.(21) The current study is the interim analysis of the first five serial patients to report early ECG changes after cardiac radioablation. This clinical trial was approved by the Institutional Review Board (No.1903-015-1014) of the participating institution (Seoul National University Hospital) and conducted in accordance with the Declaration of Helsinki.

2.1.2. Patients eligibility

Eligible patients were ≥ 19 years old and had more than two documented VT episodes on ECG and/or ICD therapy (shock or ATP) deliverer due to sustained VT within 6 months or cardiomyopathy (left ventricular ejection fraction < 50%) related to monomorphic premature ventricular contractions (PVCs > 15%) prior to study enrollment. The study candidate should have been

performed standard therapy for VT including antiarrhythmic drugs (unable to adapt to antiarrhythmic medications or uncontrolled even after 2 months of adequate treatment) or catheter ablation (previous failed catheter ablation for VT or were not suitable for catheter ablation due to left ventricular thrombosis, severe lung disease, vascular abnormality, heart malformation, etc.). Patients were deemed ineligible if the left ventricular ejection fraction was under 15%. Patients were also ineligible if their life expectancy was under 1 year due to underlying disease except VT

2.1.3. Targeting and treatment (radiotherapy)

A synthesis of imaging studies, 12-lead ECG, and electrophysiological mapping were used to localize the treatment target (arrhythmogenic substrate on ventricular myocardium) for SBRT. The use of imaging techniques was not limited, and determined by the responsible physician. If the patients had previous catheter ablation history, the three-dimensional electroanatomical mapping (CARTO® 3 electroanatomical mapping system, Biosense-Webster, Diamond Bar, CA, USA), for VT was the primary guide for SBRT.

Patients received a single dose of 25 Gy delivered with SBRT to the arrhythmogenic substrate as defined in the previous clinical trial and reports.(5, 22) The Eclipse^{TM} system (Varian

Medical Systems, Palo Alto, CA) was used for treatment planning, and volumetric modulated arc therapy planning was performed using three half arcs with a 10 MV flattening filter-free beam. The Varian TrueBeam linear accelerator (Varian Medical Systems, Palo Alto, CA, USA) was used for cardiac radioablation.

2.2. Results

2.2.1. Patients demographic features

From September 2019 to November 2020, total five patients were treated with noninvasive SBRT for their intractable VT. The mean age was 74 (range, 67 to 85), and two of five patients were female.

[Table 1] Patient characteristics

Variable	Case 1	Case 2	Case 3	Case4	Case 5
Age (yr)	72	67	73	85	72
Sex	Male	Female	Female	Male	Male
BMI (kg/m^2)	30.4	22.9	21.9	25.4	24.7
NYHA class (1 mo. before SBRT)	III~IV	II	II	III~IV	III
LVEF	24 %	57 %	36 %	26 %	27 %
Hypertension	Yes	No	No	Yes	Yes
Diabetes	Yes	Yes	No	No	No
CKD	Yes	No	No	No	No
antiarrhythmic drugs	Yes	Yes	Yes	Yes	Yes
No. of previous					
RFCA	1	2	1	0	1
PCI	0	0	0	0	1
OHS	1	0	0	3	0
Cardiomyopathy type	Non-ischemic	Non-ischemic	Non-ischemic	Ischemic	Ischemic

BMI, body mass index; SBRT, stereotactic body radiation therapy; VT, ventricular tachycardia; NYHA, New York Heart Association; PVC, premature ventricular complex; LVEF, left ventricular ejection fraction;

CKD, chronic kidney disease; RFCA, radiofrequency catheter ablation; PCI, percutaneous coronary intervention; OHS, open heart surgery; ICD, implantable cardioverter defibrillator

2.2.2. Case 1

A 72-year-old man was diagnosed with sustained VT originating from anterior right ventricular outflow tract area confirmed by 3-dimensional electroanatomical mapping. Radiofrequency catheter ablation was performed, but was not effective. The patient was hemodynamically unstable due to sustained VT. Therefore, noninvasive cardiac radioablation was considered for the patient. After 2 days from radiotherapy, the VT was dramatically suppressed, and there was only non-sustained form of VT till post-RT day 9. Except four episodes of VT recurrences within 2 weeks, there was no VT episodes after post-RT day 17. Interestingly, there was a notable change in VT morphology and cycle length. At post-RT day 1, the patient's VT morphology was not changed with same tachycardia cycle length (TCL). However, VTs did not last any longer than 5 or 6 beats of run. At post-RT day 3, the TCL was prolonged with QRS morphology changed (Figure 1).

[Figure 1] Ventricular tachycardia cycle length changes after SBRT

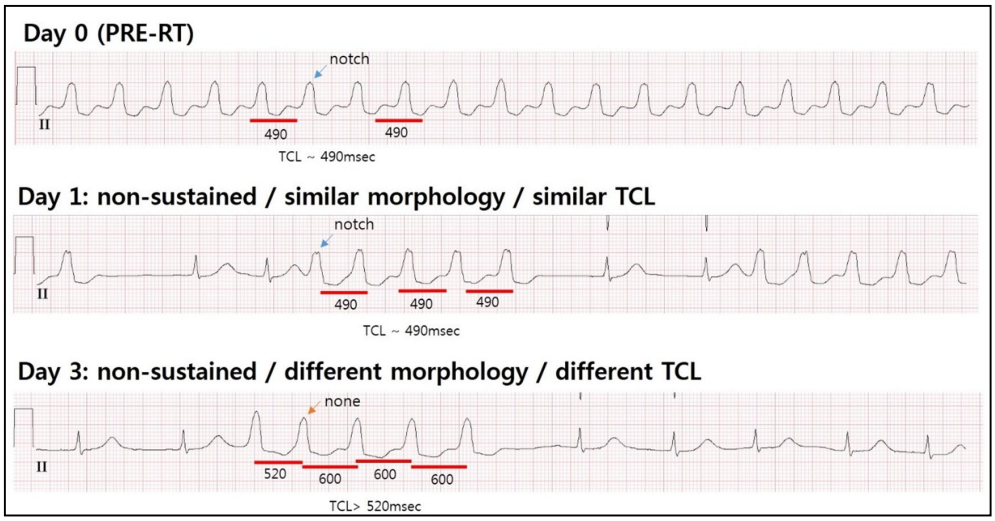

SBRT, stereotactic body radiotherapy TCL, tachycardia cycle length; PRE-RT, pre-radiotherapy;

2.2.3. Case 2

A 67-year-old woman was diagnosed with exercised induced sustained VT during treadmill test. The patient always experienced dizziness with recurrent syncope during exercise. The 3-dimensional electroanatomical mapping was performed and the VT was confirmed to come from left ventricular summit area. The sufficient antiarrhythmic drug and radiofrequency catheter ablation were tried, but were not effective. Therefore, noninvasive cardiac radioablation was considered for this patient. The PVC and VT burden was decreased immediately after radiotherapy during continuous ECG monitoring (Figure 2).

[Figure 2] Decreased PVC/VT burden after radiotherapy

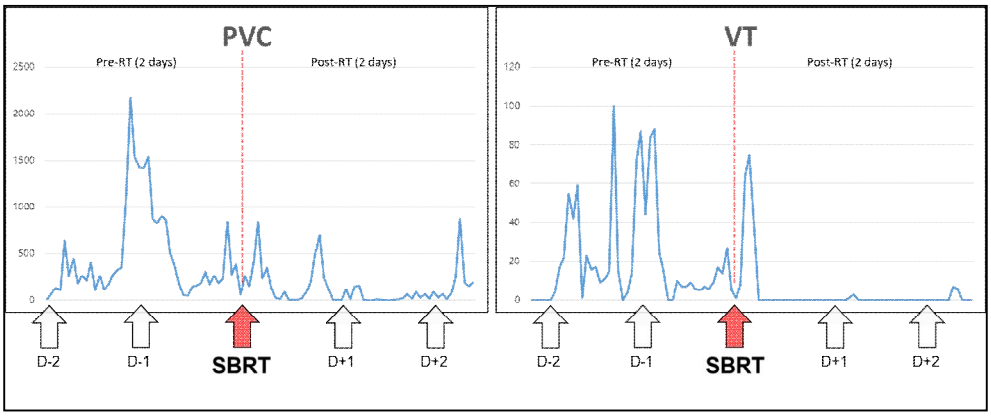

SBRT, stereotactic body radiotherapy; PVC, premature ventricular complex; VT, ventricular tachycardia

Unlike the case 1, the VT morphology was not significantly changed after irradiation. The VT rate was slightly accelerated immediate post-treatment, and decelerated afterwards (Figure 3).

[Figure 3] Pre- and post-RT VT morphology and rate changes

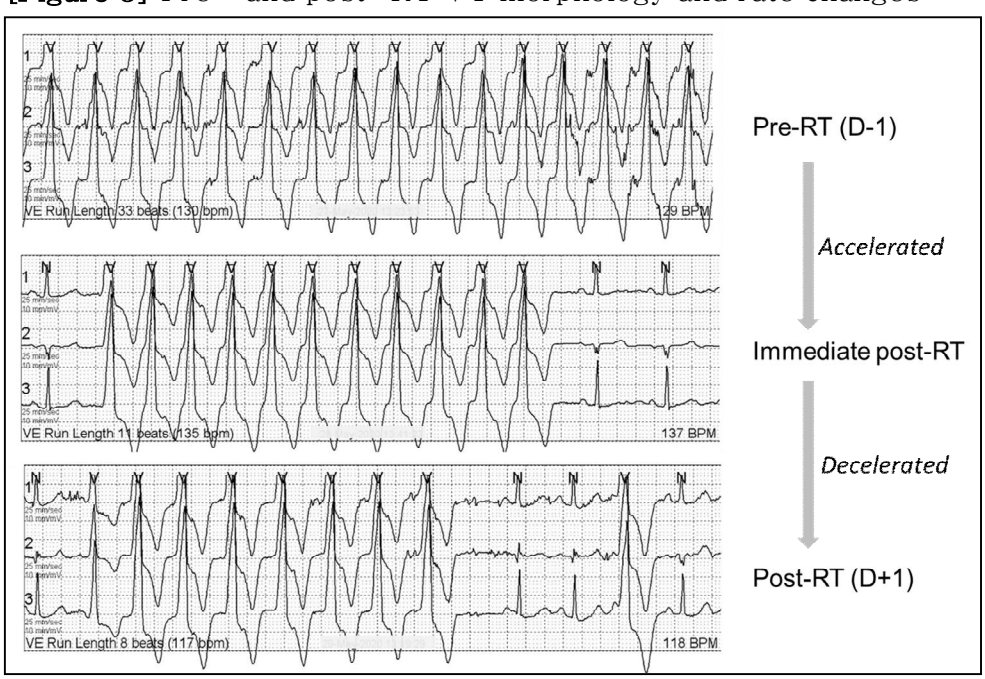

RT, radiotherapy

2.2.4. Case 3

A 73-year-old woman was diagnosed with PVC induced cardiomyopathy with left ventricular ejection fraction of 36%. The PVC was originated from left ventricular summit area confirmed by 3-dimensional electroanatomical mapping. Radiofrequency catheter ablation was performed, but was not effective. The patient was intolerable to antiarrhythmic treatment because of drug side effects. Therefore, noninvasive cardiac radioablation was considered for this patient. Within 24 hours after radiotherapy, the PVC burden was decreased by 59.9%. The coupling interval PVC was slightly prolonged from immediate post-RT (Figure 4).

[Figure 4] Pre- and post-RT Coupling interval changes

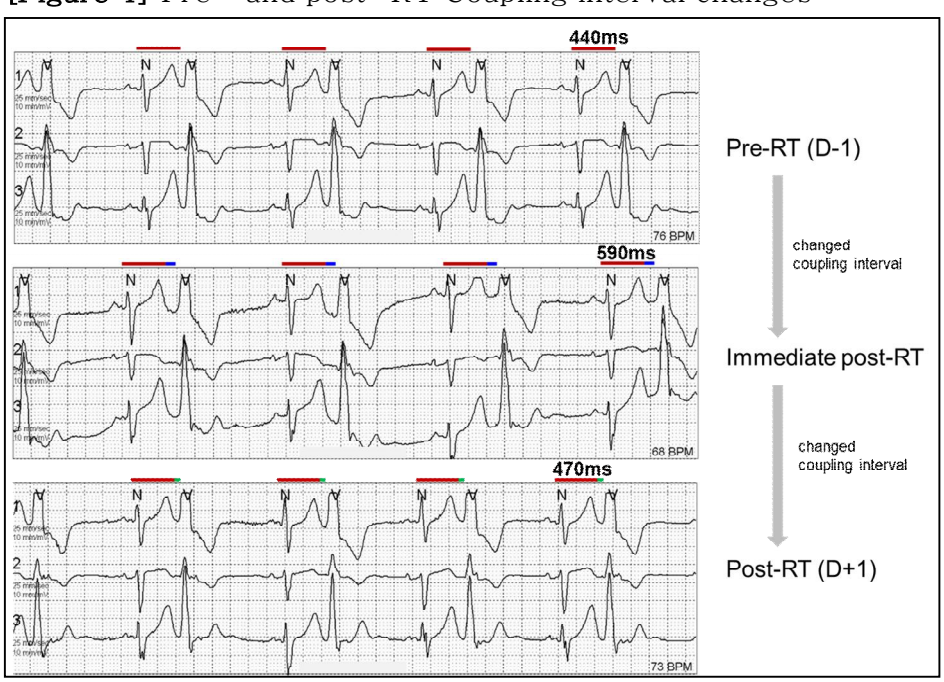

RT, radiotherapy; 1D, 1day

2.2.5. Case 4

An 85-year-old man was diagnosed with sustained VT originating from the mid-inferior myocardial scar of the left ventricle during optimal medical treatment. The catheter ablation was contraindicated for this patient, owing to the previous medical history of multiple aortic and mitral valvular replacement surgeries. Therefore, noninvasive cardiac radioablation was considered for the myocardial scar at the inferior part of the left ventricle. Within 24 hours after radiotherapy, both ventricular arrhythmias burden decreased by 51.8% and 46.4%, respectively (Figure 5). The patient received only one antitachycardia pacing (ATP) therapy for sustained VT by the ICD on the second day after radiotherapy. After 3 days of radiotherapy, no ICD therapy (ATP or shock therapy) was performed for 3 months.

[Figure 5] Disappeared VT episodes after radiotherapy

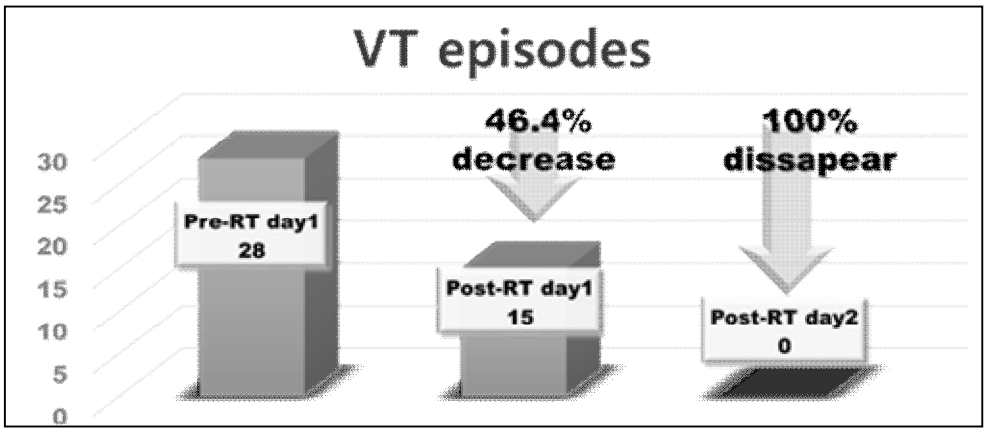

VT, ventricular tachycardia; RT, radiotherapy

2.2.6. Case 5

An 85-year-old man, who had performed percutaneous coronary intervention on left anterior descending (LAD) artery due to non-ST-elevation myocardial infarction had a large scar on entire mid to distal LAD territory with apical aneurysm. He admitted via emergency department due to recent repetitive ICD therapy (10-20 times/day). He had catheter ablation, but numerous VTs with various morphology and hemodynamically instability were observed. After ablation, he had LV mural thrombus, and could not try another ablation. Therefore, noninvasive cardiac radioablation was considered. The target for radioablation was large infarcted area based on 3-dimensional electroanatomical mapping and MRI finding (large scar from mid septum to apex with aneurysmal dilatation of apical segment), During the 2 days before radiotherapy, there were fifteen ICD therapies performed (ATP #9 and shock #6). During 2 days from immediate after SBRT, there was no sustained VT events needed ICD therapies.

2.3. Discussion

In these five cardiac radioablation cases, we observed an early VT suppression response. Interestingly, VT or PVC characteristics (cycle length, morphology, and coupling interval) also changed immediately after cardiac radioablation. Although

clinical evidence for the acute or early response of VT to cardiac radioablation is limited in both quantity and quality, the results of these five cases show that radioablation could be a promising treatment modality for urgent patients with incessant VT. Therefore, further research regarding the mechanism of the early antiarrhythmic effects of cardiac radioablation is crucial.

.

Chapter 3. Mechanism study for early antiarrhythmic effect of cardiac radioablation : early changes in rat heart after high dose irradiation

3.1. Methods

3.1.1. Study approval

All animal experiments in this study were approved by the Institutional Animal Care and Use Committee of Seoul National University Hospital (approval number: 18-0245-S1A1). Animals were maintained in a facility accredited by AAALAC International (#001169) in accordance with the Guide for the Care and Use of Laboratory Animals 8th edition, NRC.

3.1.2. Animals

Male 9- to 10-week-old wild-type Lewis rats (OrientBio, Sungnam, Korea) (n=95, weighing 300-400 g) were used in this study, including 10 rats in the control group. Different irradiation doses (20, 25, 30, 40, or 50 Gy) were administered. Animals were sacrificed for heart explantation on day 1 and weeks 1, 2, 3, and 4, respectively. Electron microscopic evaluation was performed in the 30 Gy group at various time points for representative, as there was significant difference in histological changes between 20 Gy/25 Gy and 30 Gy group in the pilot experiment. Body weight, left

ventricular dimensions, echocardiography, and electrocardiography were measured at baseline, day 1, and weeks 1, 2, 3, and 4. Three non-irradiated rat hearts were explanted at 1- or 2-weeks as a control group.

3.1.3. Irradiation

Rats were randomly divided into six radiation dose groups (a single dose of 0, 20, 25, 30, 40, and 50 Gy groups, respectively). Rats were anesthetized with Zoletil (0.04-0.06 mL/kg, I.M.) before irradiation and fixed in a customized acrylic jig. Before irradiation, a CT scan was performed using The Brilliance Big Bore™ CT simulator (Philips, Cleveland, OH, USA) with 1-mm slice thickness. CT simulation-based planning was conducted with Eclipse™ (Varian Medical Systems, Palo Alto, CA) to evaluate radiation dosage to the whole heart, lung, and esophagus (**Figure 6**). Rats were placed in a prone position. Parallel-opposed lateral fields with half-beam blocking were used to cover the whole heart and shield the posterior lungs. A 90% isodose was administered to cover 100% of the heart. Clinac iX (Varian Medical Systems, Palo Alto, CA) was used for irradiation. Radiation was delivered at a rate of 6 Gy/min.

[Figure 6] Treatment plan

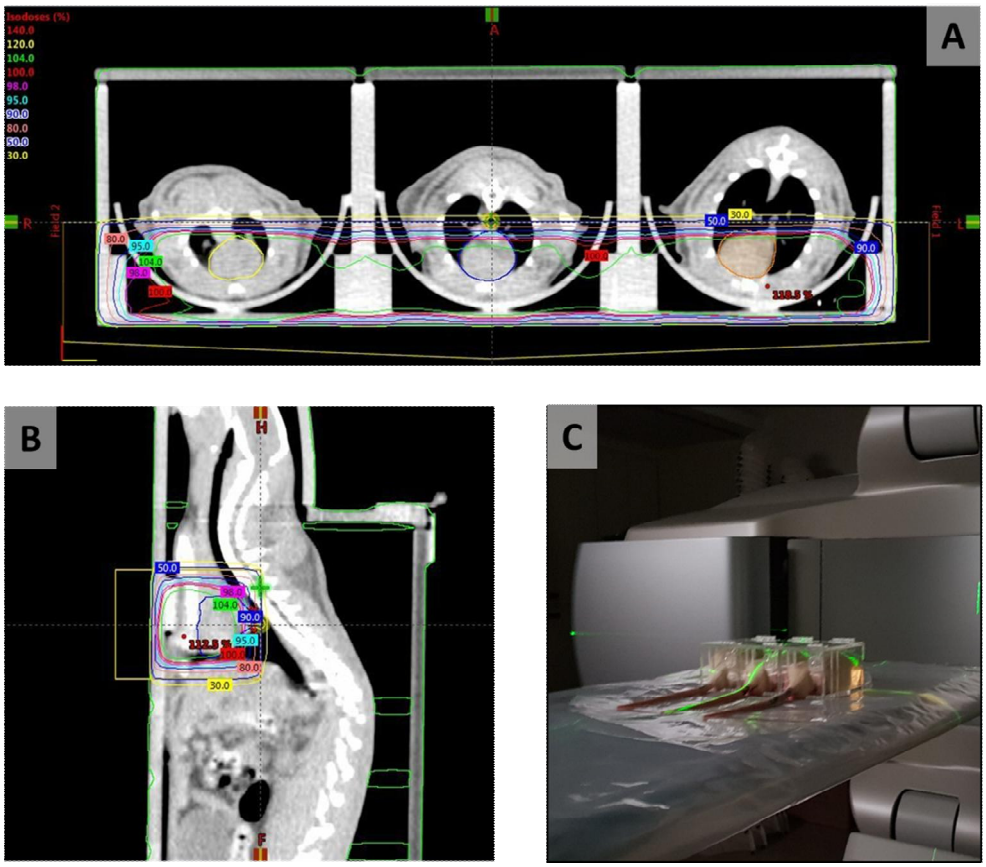

Simulation CT was taken under prone position for the planning. Hearts in each rat were delineated. Parallel beams with half beam block principles were used. (A) Dose distributions in axial and (B) sagittal view. (C) Customized jig was used for immobilization.

3.1.4. Experimentation and harvesting

Rats were sacrificed after irradiation at day 1 and weeks 1, 2, 3, and 4. Rats were anesthetized with Zoletil (0.04–0.06 mL/kg, i.m.) and maintained with isoflurane (4% for induction; 2–3% for maintenance). Body weight measurement, electrocardiography, and echocardiography were performed. Blood was replaced with heparinized saline (0.2 units/mL) perfused rapidly from the

posterior vena cava. Explanted hearts were fixed for 24 hours in 4% paraformaldehyde solution in 0.1 M phosphate buffer.

3.1.5. Staining

Following dehydration and embedding in paraffin, serial 4-μm sections were cut in the coronal plane showing all four chambers and His-bundle area. Sections were stained with hematoxylin and eosin (H&E) and Masson's trichrome (MT) for histopathologic evaluation. For immunohistochemical analysis, paraffin blocks were re-cut and stained with anti-C4d (#MA5-18044), anti-CD3 (#14-0037-82), anti-CD34 (#MA5-18091), anti-CD68 (#MA5-13324), and anti-Des (#MA5-13259) antibodies (Thermo Fisher Scientific, Waltham, MA, USA). The anti-connexin-43 (Santa Cruz) and anti-α-sarcomeric actin (Sigma) probed with Alexa Fluor 488 (anti-connexin-43) /555 (anti-α-sarcomeric actin) anti-mouse secondary antibody were used for immunofluorescence staining and DAPI for nuclear counterstaining. The cells were analyzed using confocal microscopy (LSM710; Zeiss, Oberkochen, Germany) and Leica Application Suite X software. TUNEL assay was conducted to detect cellular apoptosis using a TUNEL kit (#S7101, EMD Millipore Corporation, Darmstadt, Germany). Slides were scanned using Aperio AT2 (Leica

Byosystem, Inc., IL, USA) for virtual slides and were analyzed with ImageScope software version 12.4 (Aperio Technologies, Inc., CA, USA). To evaluate C4d deposition on myocardium, an automated image analysis algorithm Aperio Positive Pixel Count v9 using a default set of parameters was used as described previously.(23) Interpretation of C4d positivity was performed according to the ISHLT-WF-2013 guidelines.(24)

3.1.6. Electron microscopy

Tissue specimens from five different locations (left/right atrial appendage, left/right ventricular free wall, and interventricular septum) were fixed and processed using JEM-1400 transmission electron microscopy (JEOL, Japan) as described by Cocchiaro et al.(25) Standard transmission electron microscopy and immuno-electron microscopy were performed. Digital images of sequential fields were collected for ultrastructural analysis.

3.1.7. Electrocardiography and echocardiography

Electrocardiography (ECG) and echocardiography were performed at baseline pre-irradiation and on harvest day. ECG rhythm strip was monitored and recorded by Power Lab (AD Instruments, Sydney, Australia). Parameters (heart rate, PR

interval, and QRS duration) were measured using LabChart Reader version 8.0 (AD Instruments, Sydney, Australia). Average values of 10 measurements of randomly selected beats during 1-minute recording were determined. The Bazett's formula normalized to average rat RR (QTc(n)=B=QT/(RR/f)(1/2), f=150ms) was used for QT correction.(26) Echocardiography was performed for cardiac structural and functional evaluation using Toshiba Aplio XG SSA- 790A (Toshiba Medical Systems, Tokyo, Japan) with a sector probe (Toshiba PST-65AT transducer). Cardiac short axis M-mode recordings at the mid-left ventricular level were used to obtain ventricular ejection fraction.

3.1.8. Statistical analysis

Data are presented as mean ± SEM. Statistical differences between groups were analyzed by analysis of variance (one-way ANOVA), followed by Tukey's multiple comparisons test or Dunnett's test. *P* values less than 0.05 were considered statically significant.

3.2. Results

3.2.1. High-dose irradiation response: pathologic observation

Cardiac myocardium remained intact without rupture or

destruction throughout the observation period. The surrounding pericardium was visually normal without effusion. Cardiac valves were intact. No evidence of intracardiac thrombus or coronary artery stenosis was observed. Cardiac myofibrillar arrangement was well preserved with intact Z- and M-lines on electron microscopy without myofibrillar rupture or discontinuity. To assess myocyte injury after high dose irradiation, anti-C4d staining and TUNEL assay were performed. No evidence of myocyte necrosis or apoptosis was noted (Figure 7). Nuclear size was not significantly altered.

[Figure 7] H&E and IHC staining on ventricular myocyte irradiated with 30 Gy at 4 weeks.

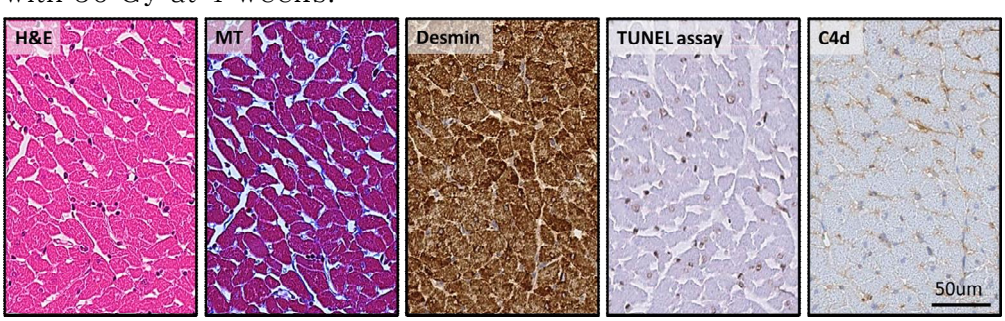

Irradiated left ventricular free wall subendocardium of rats was stained with hematoxylin and eosin (H&E), Masson's trichrome, and immunohistochemistry (Desmin, TUNEL assay, and C4d immunostaining). Myocyte necrosis and apoptosis were not observed in rat hearts irradiated by 20-50 Gy. Intercellular space (interstitium) was widened but not fibrotic. Cellular rupture and destruction of myocytes were not observed. ×400 Magnification.

Intercalated discs were widened, with perturbed cellular connections between adjacent cardiac myocytes (Figure 8). Sporadic focal bulging and multiple gap junction vesicles of variable sizes were noted close to damaged intercalated discs. Longitudinal continuity of intercalated discs was maintained. At week 4, intercalated disc lining was twisted and thickened relative to baseline on both atrial and ventricular sides. The incidence did not vary according to timing of observation or location. In the immunofluorescence staining of connexin-43, I observed a decreased expression of connexin-43 at 2 or 3 weeks, but slightly increased at 4 weeks (Figure 9).

[Figure 8] Electron microscope examination of the left ventricular myocardium of irradiated rat heart (30 Gy single fraction)

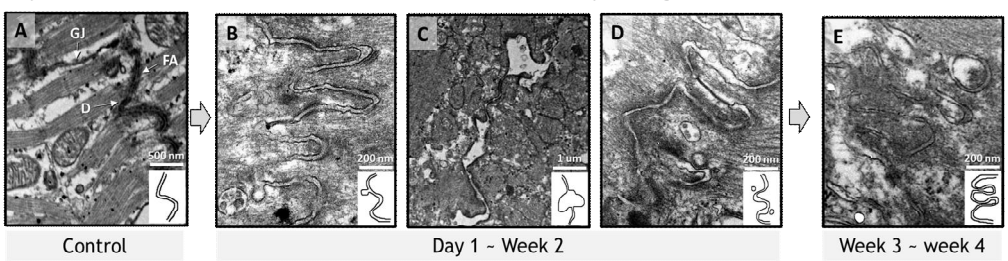

Compared to normal intercalated discs (A), irradiated intercalated discs exhibited irregular widening focal protrusion (B) or segmental separation (C) peaking at 1-week. These abnormalities were observed in 30 Gy-irradiated rats harvested at day 1 and were rarely observed after week 2. From week 2, intercalated discs exhibited irregularly widened longitudinal cell connections with adjacent gap junction vesicles (D). Damaged intercalated discs were narrowed after 3 weeks. Remodeling was uneven and twisted (E) (x50,000 magnification)]

[Figure 9] Immunofluorescence staining of connexin-43

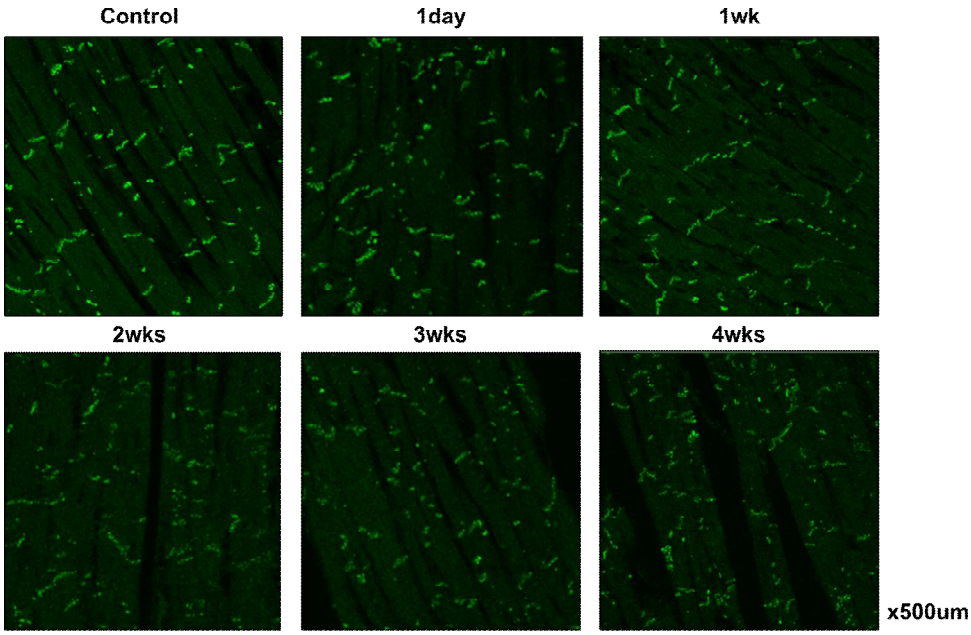

Diffuse vacuolization and loosened myocardial architecture were noted (Figure 10). Vacuolization observed in H&E staining comprised interstitial edema and intracellular swelling on transmission electron microscopy (Figure 11). These effects were dose-dependent, peaked at 3 weeks, and were reversed at 4 weeks. The vacuolization area per high-power field increased with radiation dose. Immunohistochemical staining revealed CD68 immunopositivity in the interstitial area corresponding to regions of vacuolization, indicating macrophage/mononuclear interstitial infiltration into interstitial vacuoles. C4d immunopositivity on vacuolization was less prominent in the His-bundle area than in

atrial or ventricular myocardial areas (Figure 12).

[Figure 10] Interstitial vacuolization

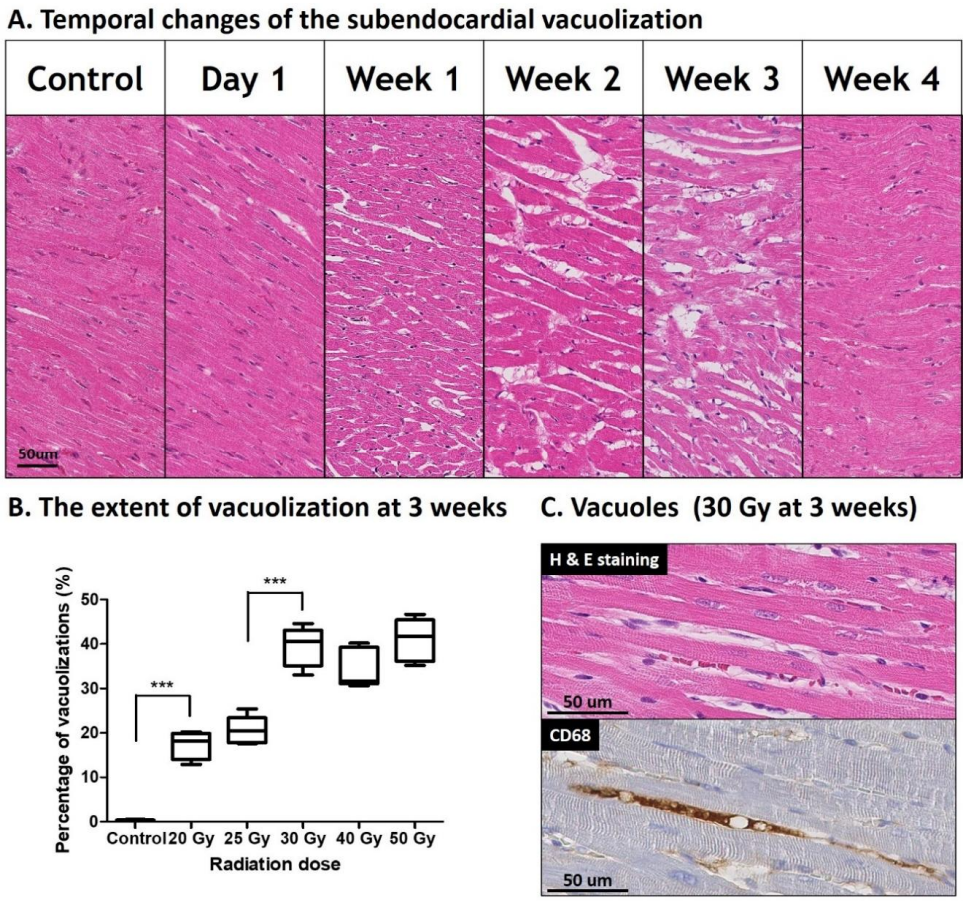

A: Temporal changes of the left ventricular subendocardial vacuolization. x400 Magnification. B: Boxplot of the percentage of vacuolization at 3 weeks according to radiation dose. The extent of vacuolization was measured at left ventricular subendocardium using Aperio Imagescope (Leica). All groups were statistically different from each group, except 20 and 25 Gy group and 30, 40, 50 Gy group. *** indicates $p<0.001$ C: The vacuolized area on H&E staining showed positive staining for CD68. ×400 Magnification.]

[Figure 11] Interstitial and cytoplasmic edema after irradiation

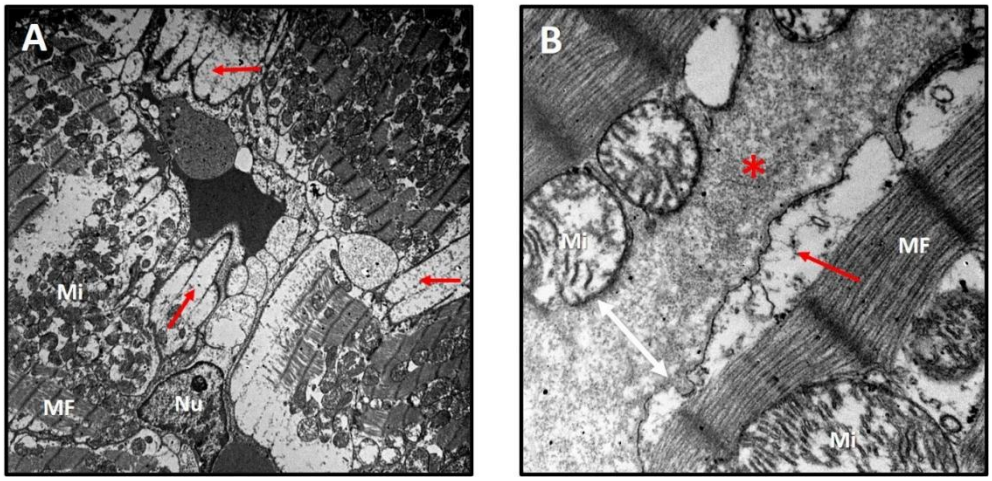

A: Rat left ventricular mid-myocardium on electron microscopy (x5,000 magnification). B: Rat left ventricular mid-myocardium on electron microscopy (x40,000 magnification), left ventricle irradiated with 30 Gy (3 weeks). Cellular membranes were dilated due to cytoplasmic swelling (red arrows). Interstitial edema widened intercellular spaces (red asterisks and white arrow). Subsarcolemmal and interfibrillar mitochondria (marked as 'Mi') were damaged and variable in size. Myofibrils with Z- and M-lines were intact. No remarkable abnormalities in myocyte nuclei (marked as 'Nu') were noted.]

[Figure 12] Positivity of C4d deposition on interstitial vacuolization

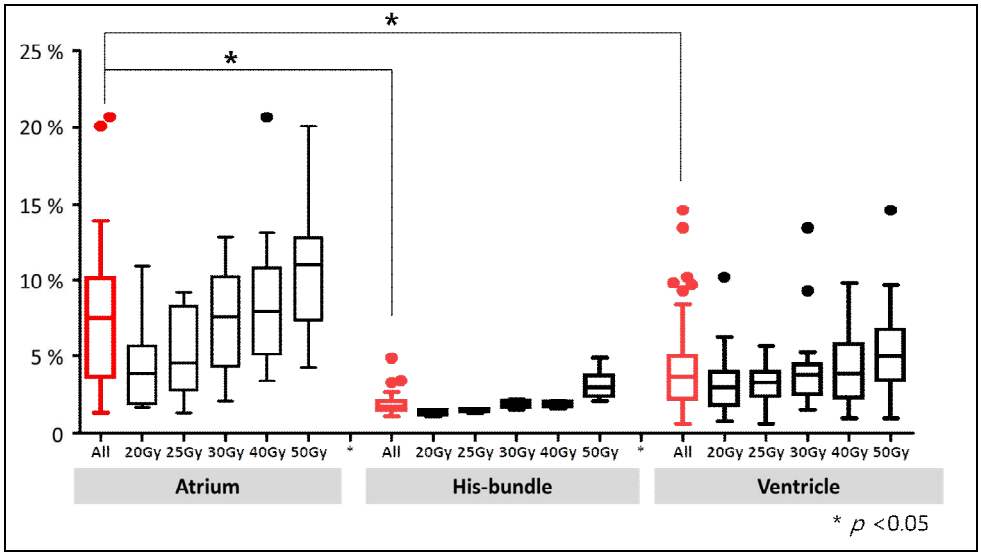

Capillary diameter was markedly dilated after week 2, potentially leading to microvascular extravasation and resultant interstitial swelling. Anti-CD34 immunostaining of capillaries did not reveal alterations in capillary number or evidence of capillary apoptosis based on TUNEL assay (**Figure 13**). Red blood cells were attached to capillary vessel walls. Neutrophil infiltration was scarce. Intracellular structural damage including cytoplasmic swelling and mitochondrial damage contributed to intracellular vacuolization (**Figure 14**). Cytoplasmic swelling was accompanied with sarcomere and sarcoplasmic reticular swelling, resulting in increased intermyofibrillar space with intracellular reticular pattern of individual myocytes. Intracellular mitochondrial damage included mitochondrial rupture, fission, or fusion. Mitophagy was noted, indicating mitophagosis of damaged mitochondria. This change was prominent from week 2 and was partially resolved at week 4.

[Figure 13] Myocardial capillaries

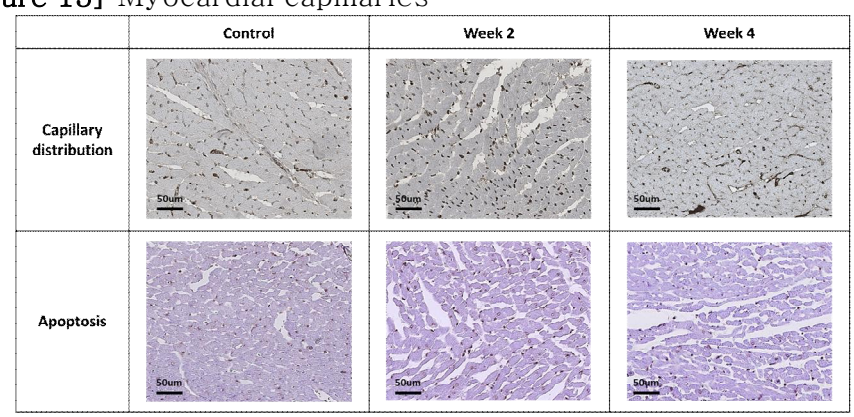

[Figure 14] Intracellular edema with prominent mitochondrial damage

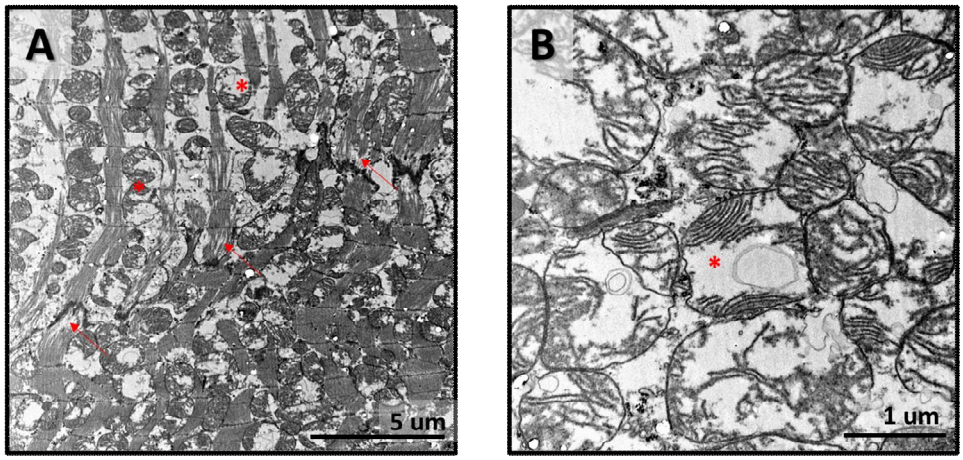

(A) rat heart, ventricular myocardium, electron microscopy (Mag x8,000). (B) rat heart, ventricular myocardium, electron microscopy (Mag x30,000), left ventricle irradiated with 30Gy (2 weeks). The inter-myofibrillar widening without discontinuation was marked with red arrows in Panel A. A number of mitochondria were broken and could not maintain their normal shape (Panel B).]

Myocardial endo- and epicardial lining was thickened with prominent hyperplasia and interstitial edema (Figure 15). Intracardiac coronary arteries and arterioles exhibited intimal proliferation and peri-vascular edema beginning from 20 Gy/2-weeks in a dose- and time-dependent manner (Figure 16). Fibroblast and inflammatory cell recruitment were noted between loosened externa. No obvious histopathologic damage was noted in cardiac valvular structures and pericardium. The main observations are depicted in Figure 17.

[Figure 15] Atrium (Left atrial appendage)

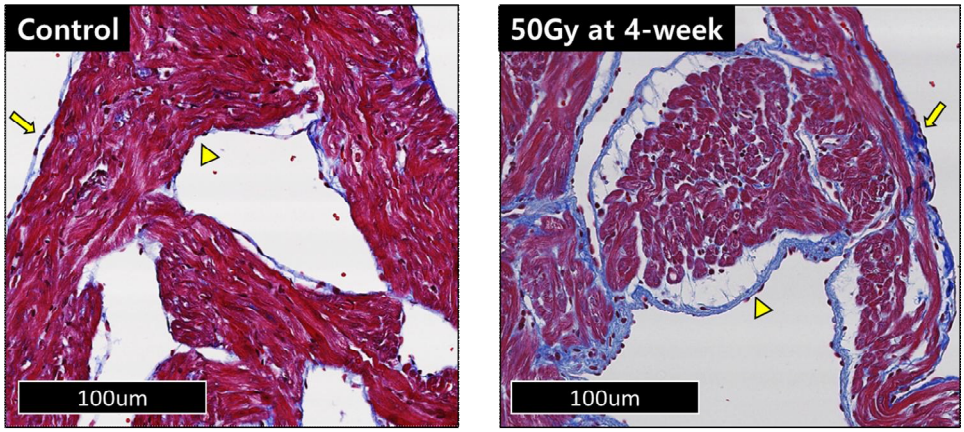

Compared to control tissue (left), left atrial appendage (right) irradiated with 50 Gy showed endo-(arrow head) and epi-cardial (arrow) thickening with prominent hyperplasia and interstitial edema. Atrial myocardium also showed myocardial vacuolization most prominent at 3-week and regressed at 4-week. This changes are not definite at 2-week, but at 3-week grossly prominent from 20 to 50 Gy.

[Figure 16] Intramyocardial coronary artery

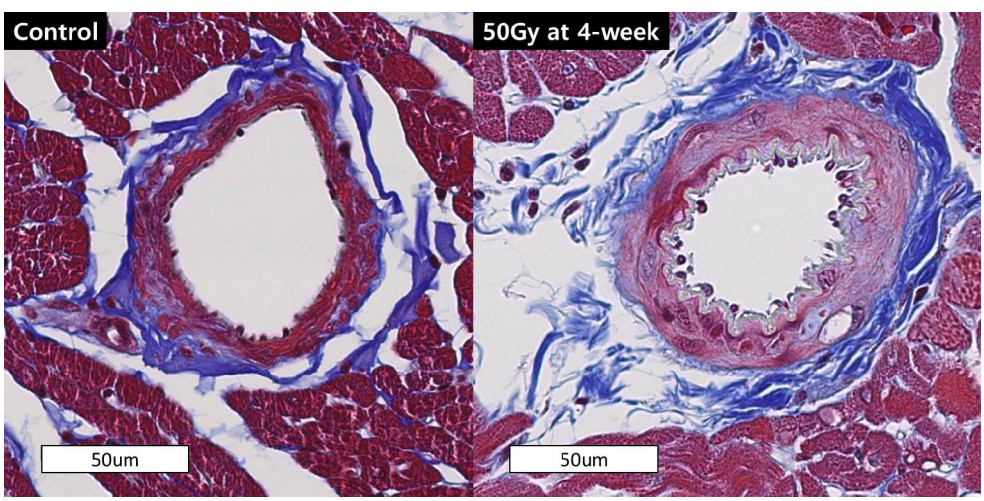

Rat heart, coronary artery. 50Gy/4-week. intimal proliferation and peri-vascular edema starts from 20Gy/2-week with dose/time-dependant manner. Recruitment of fibroblast or inflammatory cells between loosened externa.

[Figure 17] Main histopathologic findings.

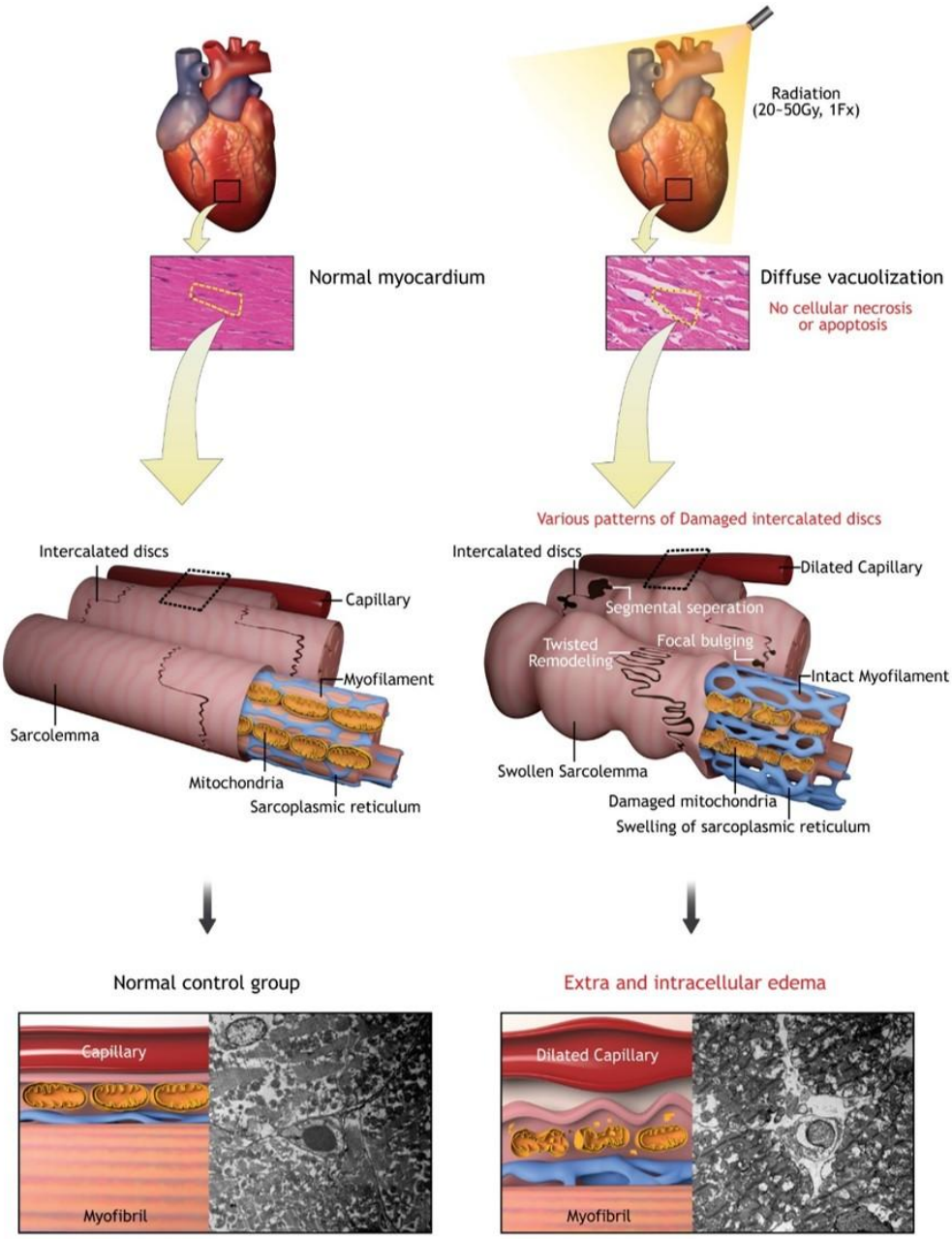

Irradiated rat heart myocardium (right) and normal rat heart myocardium (left) were compared. No cellular necrosis or apoptosis after irradiation was noted. Diffuse vacuolization was correlated with interstitial and sub-sarcolemmal edema. Intercalated discs between myocytes were widened with diverse patterns.

3.2.2. Electrocardiography

Detailed ECG parameters (heart rate, PR interval, and QTc interval) and ST-segment changes after irradiation are presented in Figure 18.

[Figure 18] Electrocardiographic changes.

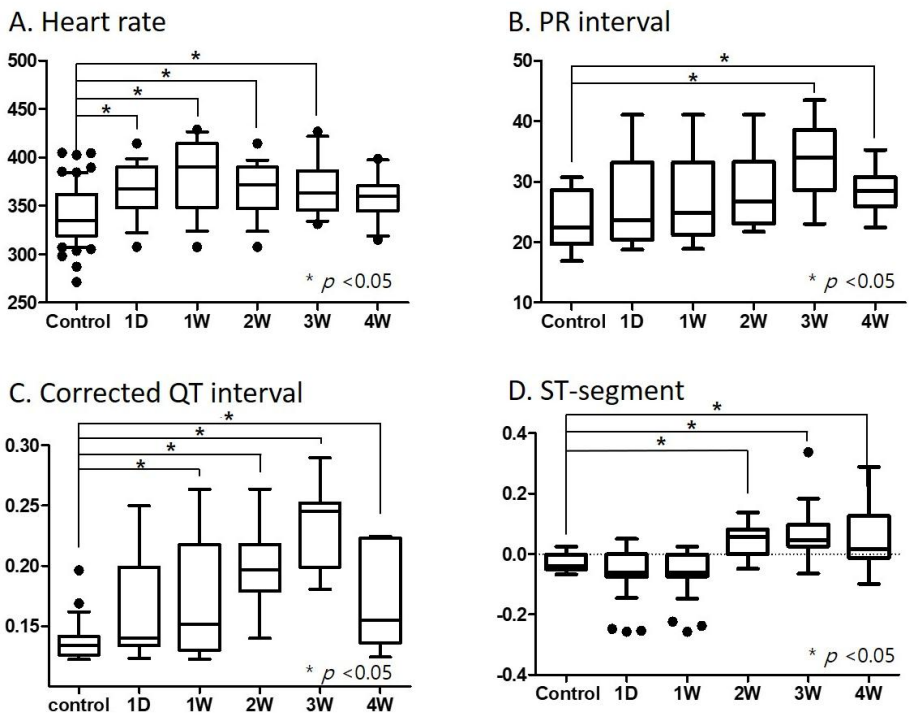

Resting heart rate was increased after irradiation. The PR interval, representing the conduction velocity from atrium to ventricle, was slightly delayed after 2 weeks. The corrected QT interval, representing intraventricular conduction properties, was prolonged relative to baseline. The ST-segment was depressed

after irradiation but significantly elevated after 2 weeks in most cases. No clinically significant abnormal tachy- or brady-arrhythmias were noted in all dose groups. Occasional atrial premature beats were observed in rats irradiated with 40 Gy or 50 Gy at 2-4 weeks, which were absent in lower dose groups.

3.2.3. Echocardiography results

No significant effects of irradiation on left ventricular ejection fraction were observed (Figure 19). No pericardial effusion or intracardiac thrombi were observed. Left ventricular chamber size and wall thickness were within the normal range. Cardiac valvular motion was visually normal.

[Figure 19] Echocardiographic images of rat heart after 50Gy irradiation.

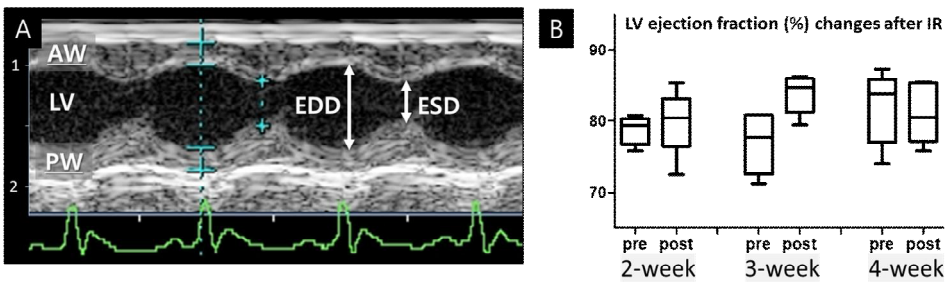

Left ventricular wall thickness and ejection fraction derived by M-mode echocardiography were preserved after irradiation even at 4-week (Panel A). Compared to baseline LVEF (%) before irradiation, there was no statistical significant difference after irradiation at 2-, 3-, and 4-week (Panel B). There was no evidence of wall motion abnormality, valvular dysfunction, pericardial effusion or intracardiac thrombus. LV, left

ventricle; AW, anterior wall; PW, posterior wall; EDD, end-diastolic dimension; ESD, end-systolic dimension; LVEF, left ventricular ejection fraction (100xESD/EDD); IR, irradiation]

3.2.4. Body weight and laboratory test results

Body weights decreased during follow-up after irradiation, especially in the 40 and 50 Gy group after 3 weeks. White blood cell counts were decreased at 1 week but subsequently normalized. Neutrophil proportion was slightly increased after irradiation. Body weights and laboratory data are presented in Figure 20.

[Figure 20] Body weight and laboratory data

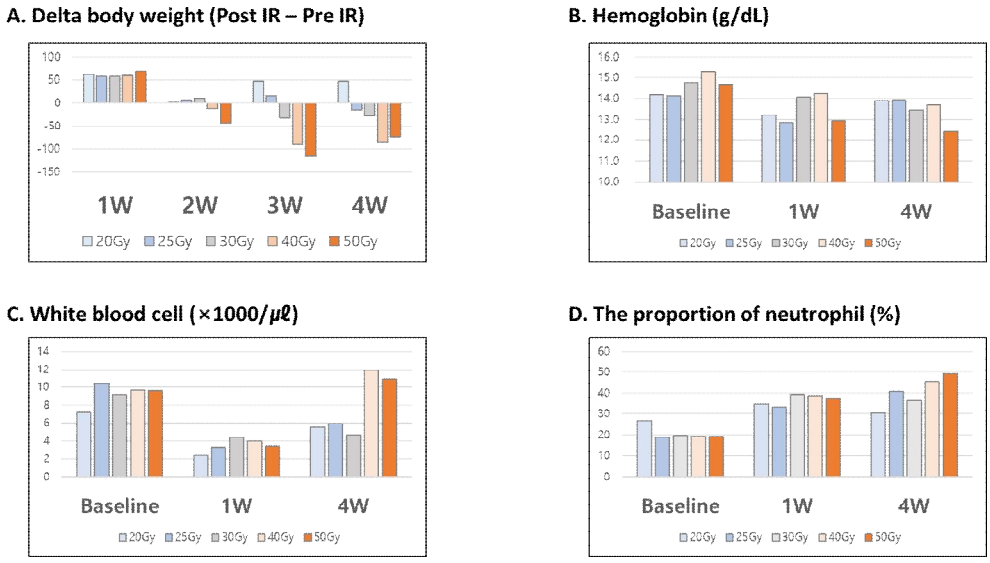

3.3. Discussion

In this study, I assessed the effects of high-dose irradiation of rat heart. High-dose irradiation resulted in widening of intercalate discs, intracellular cardiac sarcotubular system edema, extracellular swelling, and diffuse mitochondrial damage without definite myofibrillar disruption. This study demonstrated corresponding ECG changes including intracardiac conduction delay with ST-segment changes. With regard to cardiac arrhythmias, the present study is the first to suggest that cell-to-cell conduction disturbances and cellular membrane potential alterations result in early electrophysiological changes after cardiac radioablation.

Most preclinical and clinical studies on cardiac effects after irradiation have examined radiation-induced heart disease based on autopsy findings of myocardial fibrosis after massive radiotherapy in humans (27). Recently, the relationship between cardiac toxicity and RT has also been studied in cancer patients, high-dose irradiation increased coronary disease.(28) In previous Although pioneering research included early cardiac responses after IR, the clinical importance of early changes was less significant than that of late changes, as they were not prominent in light microscopy and ultrastructural changes were largely reversible.(18-20, 29) Most early studies used doses of 10 to 20 Gy. Recently, Kiscsatari et al.

performed an in vivo study in rat hearts using the same doses as those in my study, However, their study focused on radiation toxicity in the heart, and tissue was harvested at week 19 (30). They reported that fibrosis was present in groups irradiated with 40 Gy or more at 19 weeks after irradiation.

Based on prior preclinical studies demonstrating radiation-induced cardiac fibrosis, there have been several attempts to test the feasibility of radiotherapy for arrhythmias, mainly targeting pulmonary vein isolation for atrial fibrillation (10, 31-34). Sharma et al. described pathologic changes in targets at the cavotricuspid isthmus, AV node, pulmonary vein–left atrial junction, and left atrial appendage of mini-swine on 25 to 196 days after radiation (33). Further, the authors reported discrete fibrosis with elongated fibroblasts, which was not observed in the early phase after radiation. Rapp et al. reported pathological changes in cardiomyocytes in a swine model, revealing vascular damage, fibrosis, and vacuolization after 6 months of C-ion radiation (10). Several preclinical studies have been performed to test the feasibility of radiotherapy for pulmonary vein isolation (31, 32, 35). To interpret irradiation-induced conduction block, pathologic findings in prior studies have focused on obvious differences between irradiated areas including fibrosis and undamaged non-

irradiated areas (31–34). These preclinical studies have helped to determine the therapeutic radiation dose for arrythmias, as the results demonstrated that electrophysiological changes or fibrotic scarring were achievable at doses above 25 Gy after several weeks to months post–irradiation. Conversely, other reports demonstrated complete scarring at higher doses (32, 34, 35). Although these preclinical studies focused on atrial fibrillation, anticipated antiarrhythmic mechanisms after radioablation for VT included fibrosis in the context of arrhythmia treatment.

In general, radiation–induced fibrosis occurs several months after radiotherapy (36). However, real–world data have demonstrated antiarrhythmic effects as early as immediately after radioablation (2, 12, 37). The present study was thus conducted to elucidate the mechanisms underpinning these effects. I did not observe necrosis or apoptosis in myocardium, which differs from the results of conventional catheter ablation techniques using radiofrequency and cryo–energy. Radiofrequency catheter ablation immediately generates permanent tissue necrosis by direct resistive heating and indirect passive conductive heating.(38) Several factors influence optimal lesion formation, including conductive cooling by surrounding blood flow, size of ablation catheter tip, location of targeted substrate, and catheter

manipulation techniques, which pose limitations for radiofrequency catheter ablation. (39) With regards to cryoablation, myocardial cell freezing causes rupture and cell necrosis, eventually leading to apoptosis. Extracellular ice crystal formation contributes to mechanical cell damage causing injury to cell organelles and membranes, culminating in cell death, which results in intracellular hyperosmotic stress, volume loss, and injury to cell constituents.(40) As reported here, the early effects after cardiac radioablation are underpinned by distinct mechanisms unrelated to cellular necrosis. The cardiac radioablation dose of 25 Gy used in the clinical setting for VT results in immediate responses. The current study applied higher doses up to 50 Gy, but no evidence of cardiomyocyte apoptosis or necrosis was noted. (2, 41)

Intercalated disc widening, intracellular cardiac sarcotubular system edema, and extracellular swelling observed on electron microscopy are distinct radiation-induced features largely consistent with previous findings reported in the 1970-80s. Khan et al. reported dissociation of intercalated discs observed 24 and 48 hours post irradiation with 10 Gy and 13 Gy (19). Similarly, Cillers et al. investigated the effects of irradiation on rat heart and reported that intercalated disc damage as early as 6 hours post-irradiation which peaked at 3 weeks; these changes receded 60

days after irradiation with 20 Gy. (20) A major component of intercalated discs are gap junction channels responsible for electrical cell-to-cell propagation and arrhythmogenesis in cardiac cells.(42) Although I did not employ an arrhythmia model, we speculate that intercalated disc widening may alter electrophysiological characteristics, based on previous reports on the relationship between intercalated disc remodeling and arrhythmogenesis.(43, 44).

Another notable finding regarding cardiac conduction disturbances was myocardial inflammatory responses to irradiation as suggested by prominent intra- and extracellular swelling including sarcotubular systemic dilatation. Capillary dilation and red blood cell attachment to vessel walls strongly suggested an inflammatory process. Extravasated fluid from capillaries may have induced interstitial and intracellular edema, manifesting as prominent edematous sarcolemma and dilatated sarcoplasmic reticulum. Neutrophil infiltration and aggregation were not observed, but sporadic mononuclear cell infiltration was observed with anti-CD68 staining within interstitial swollen areas. These observations can be summarized as microvascular inflammatory responses to irradiation. After the early phase, changes would proceed to irreversible fibrosis within several months as described by previous

reports.(30, 45) I did not observe changes in conduction tissue even though I employed higher doses (up to 50 Gy) than those used in previous studies on radiation toxicity on the heart, which used doses around 20 Gy. Viczenczova et al. showed that single dose of 25 Gy irradiation resulted in compensatory up-regulated myocardial connexin-43(46-48) which could not be confirmed by my finding. I could tell that the Connexin-43 expression was disorganized after irradiation. The difference could possibly be resulted from the observation period, as the studies from Viczenczova et al. were 6 weeks after irradiation and 1 day to 4 weeks in the current study. Further research is needed on mechanism of connexin-43 expression changes.

Mitochondrial damage after irradiation has been proposed to underpin radiation-induced heart disease.(49-51) Several mechanisms including oxidative stress, transcription factor pathways such as glutathione S-transferase alpha 4/Nrf2 or peroxisome proliferator-activated receptor-α, and apoptosis have been proposed to underscore mitochondrial damage related to radiation-induced heart disease, but these remain under investigation.

No clinically significant tachyarrhythmias or conduction block were observed; however, ECG changes suggested that high-

dose irradiation affected cardiac electrophysiological properties. Although heart rate was significantly increased after irradiation, intracardiac conduction velocity was delayed. ST-segment elevation following depression was notable and is commonly observed in various cardiac diseases such as myocarditis, ischemic heart disease, or stress-induced cardiomyopathy.(52) Based on the results, it can be speculated that cell-to-cell conduction disturbances and membrane potential alterations due to inflammatory processes result in ECG changes. From these pathologic and ECG findings, early electrophysiological changes leading to antiarrhythmic effects arise from modifications in electrical characteristics of cardiac tissue driven by altered conduction properties rather than necrosis or apoptosis. Therefore, early antiarrhythmic effects after radioablation differ from late phase antiarrhythmic effects. Multiple ionic currents, transporters, signaling pathways, and their interaction in ventricular myocytes underpin the clinical manifestation of VT.(53) The study results suggest that early anti-arrhythmic effects after radioablation are related to inflammatory changes rather than fibrotic changes. Further, the radiation dose could be reduced below 25 Gy in single fraction, or fractionated radioablation could be administered for medically intractable fatal VT storm.

The current study has several limitations. First, experiments were performed in healthy rats. Although research using animal models with VT is the most desirable, it is challenging to produce homogeneous VT in all subjects. Therefore, I performed experiments in normal heart tissue with a large number of study subjects and employed cardiac conditions that were as homogenous as possible. Second, cardiac electrophysiologic properties differ between rats and humans. This study result revealed irradiation effects on normal rat heart, which may not directly reflect antiarrhythmic effects on human VT. Third, this data presented histopathological findings relating ECG changes to antiarrhythmic effects, but detailed electrophysiologic mechanisms of membrane potential alterations or cell-to-cell conduction disturbances could not be determined from histopathological observations. Further studies assessing cellular action potential and myocardial electrical propagation changes, as well as proteomics analysis constituting membrane ionic channels should be performed in the future.

Chapter 4. Conclusion

From the mechanism study on antiarrhythmic effect using rat model, I could speculate that the study observation on VT suppression after cardiac radioablation could result from the myocardial cell-to-cell conduction disturbances and cellular membrane instability without direct myocardial damage including fibrosis (54).

In the aspect of cardiac radioablation therapeutic mechanism, intercalated disc widening, diffuse interstitial vacuolization, and sub-sarcolemmal swelling with mitochondrial damage were prominent observations within 1 month after high-dose irradiation. These structural changes may be correlated with cardiac conduction property changes, resulting in intracardiac conduction velocity delay in ECG findings. These observations suggest that early antiarrhythmic effects after cardiac radioablation arise from both cell-to-cell conduction disturbances and cellular membrane instability without direct necrotic damage to myofibril arrangement, which differs from later radiation fibrosis or conventional catheter ablation.

In conclusion, understanding the possible antiarrhythmic mechanism will be crucial in delineating the patient population that should receive this noninvasive cardiac radioablation treatment. Future

endeavors in radiobiology mechanisms and clinical trial development will make this novel treatment a success.

References

1. Kavanaugh JA, Holler S, DeWees TA, Robinson CG, Bradley JD, Iyengar P, et al. Multi-Institutional Validation of a Knowledge-Based Planning Model for Patients Enrolled in RTOG 0617: Implications for Plan Quality Controls in Cooperative Group Trials. Pract Radiat Oncol. 2019;9(2):e218-e27.

2. Cuculich PS, Schill MR, Kashani R, Mutic S, Lang A, Cooper D, et al. Noninvasive Cardiac Radiation for Ablation of Ventricular Tachycardia. N Engl J Med. 2017;377(24):2325-36.

3. Gianni C, Mohanty S, Trivedi C, Di Biase L, Al-Ahmad A, Natale A, et al. Alternative approaches for ablation of resistant ventricular tachycardia. Cardiac Electrophysiology Clinics. 2017;9(1):93-8.

4. Zei PC, Mak R. Noninvasive Stereotactic Radioablation for Ventricular Tachycardia: ENCORE-VT (EP-Guided Noninvasive Cardiac Radioablation): Is the Sequel as Good as the Original? : Am Heart Assoc; 2019.

5. Cuculich PS, Schill MR, Kashani R, Mutic S, Lang A, Cooper D, et al. Noninvasive cardiac radiation for ablation of ventricular tachycardia. New England Journal of Medicine. 2017;377(24):2325-36.

6. Cvek J, Neuwirth R, Knybel L, Molenda L, Otahal B, Pindor J, et al. Cardiac radiosurgery for malignant ventricular tachycardia. Cureus. 2014;6(7):e190.

7. Loo Jr BW, Soltys SG, Wang L, Lo A, Fahimian BP, Iagaru A, et al.

Stereotactic ablative radiotherapy for the treatment of refractory cardiac ventricular arrhythmia. Circulation: Arrhythmia and Electrophysiology. 2015;8(3):748-50.

8. van der Ree MH, Blanck O, Limpens J, Lee CH, Balgobind BV, Dieleman EM, et al. 'Cardiac Radioablation-a Systematic Review'. Heart Rhythm. 2020.;17(8):1381-1392.

9. Ipsen S, Blanck O, Oborn B, Bode F, Liney G, Hunold P, et al. Radiotherapy beyond cancer: target localization in real-time MRI and treatment planning for cardiac radiosurgery. Med Phys. 2014;41(12):120702.

10. Rapp F, Simoniello P, Wiedemann J, Bahrami K, Grunebaum V, Ktitareva S, et al. Biological Cardiac Tissue Effects of High-Energy Heavy Ions - Investigation for Myocardial Ablation. Sci Rep. 2019;9(1):5000.

11. Neuwirth R, Cvek J, Knybel L, Jiravsky O, Molenda L, Kodaj M, et al. Stereotactic radiosurgery for ablation of ventricular tachycardia. Europace. 2019. ;21(7):1088-1095.

12. Jumeau R, Ozsahin M, Schwitter J, Vallet V, Duclos F, Zeverino M, et al. Rescue procedure for an electrical storm using robotic non-invasive cardiac radio-ablation. Radiother Oncol. 2018;128(2):189-91.

13. Amino M, Yoshioka K, Tanabe T, Tanaka E, Mori H, Furusawa Y, et al. Heavy ion radiation up-regulates Cx43 and ameliorates arrhythmogenic substrates in hearts after myocardial infarction. Cardiovascular research. 2006;72(3):412-21.

14. Amino M, Yoshioka K, Fujibayashi D, Hashida T, Furusawa Y,

Zareba W, et al. Year-long upregulation of connexin43 in rabbit hearts by heavy ion irradiation. American Journal of Physiology-Heart and Circulatory Physiology. 2010;298(3):H1014-H21.

15. Amino M, Yoshioka K, Furusawa Y, Tanaka S, Kawabe N, Hashida T, et al. Inducibility of ventricular arrhythmia 1 year following treatment with heavy ion irradiation in dogs with myocardial infarction. Pacing and Clinical Electrophysiology. 2017;40(4):379-90.

16. Koplan BA, Stevenson WG. Ventricular Tachycardia and Sudden Cardiac Death. Mayo Clinic Proceedings. 2009;84(3):289-97.

17. Fajardo LF, Stewart JR. Capillary injury preceding radiation-induced myocardial fibrosis. Radiology. 1971;101(2):429-33.

18. Fajardo LF, Stewart JR. Pathogenesis of radiation-induced myocardial fibrosis. Lab Invest. 1973;29(2):244-57.

19. Khan MY. Radiation-induced cardiomyopathy. I. An electron microscopic study of cardiac muscle cells. Am J Pathol. 1973;73(1):131-46.

20. Cilliers GD, Harper IS, Lochner A. Radiation-induced changes in the ultrastructure and mechanical function of the rat heart. Radiother Oncol. 1989;16(4):311-26.

21. Clinical Research Information Service[Internet]; Osong(Chungcheongbuk-do): Clinical Research Information Service [Internet]; Osong(Chungcheongbuk-do): Korea Centers for Disease Control and Prevention, Ministry of Health and Welfare (Republic of Korea); 2010; KCT0004302; Clinical feasibility study of Noninvasive

Cardiac Radio-ablation for Treatment of Ventricular tachycardia; June 24, 2019 [cited on November 30, 2020]; Available from: https://cris.nih.go.kr/cris/search/search_result_st01_kren.jsp?seq=14745
[

22. Robinson CG, Samson PP, Moore KM, Hugo GD, Knutson N, Mutic S, et al. Phase I/II trial of electrophysiology-guided noninvasive cardiac radioablation for ventricular tachycardia. Circulation. 2019;139(3):313-21.

23. Brazdziute E, Laurinavicius A. Digital pathology evaluation of complement C4d component deposition in the kidney allograft biopsies is a useful tool to improve reproducibility of the scoring. Diagn Pathol. 2011;6 Suppl 1:S5.

24. Berry GJ, Burke MM, Andersen C, Bruneval P, Fedrigo M, Fishbein MC, et al. The 2013 International Society for Heart and Lung Transplantation Working Formulation for the standardization of nomenclature in the pathologic diagnosis of antibody-mediated rejection in heart transplantation. J Heart Lung Transplant. 2013;32(12):1147-62.

25. Boerma M, Zurcher C, Esveldt I, Schutte-Bart CI, Wondergem J. Histopathology of ventricles, coronary arteries and mast cell accumulation in transverse and longitudinal sections of the rat heart after irradiation. Oncol Rep. 2004;12(2):213-9.

26. Kmecova J, Klimas J. Heart rate correction of the QT duration in rats. Eur J Pharmacol. 2010;641(2-3):187-92.

27. Rubin E, Camara J, Grayzel DM, Zak FG. Radiation-induced cardiac fibrosis. Am J Med. 1963;34:71-5.

28. Jang B-S, Cha M-J, Kim HJ, Oh S, Wu H-G, Kim E, et al. Heart substructural dosimetric parameters and risk of cardiac events after definitive chemoradiotherapy for stage III non-small cell lung cancer. Radiotherapy and Oncology. 2020;152:126-132.

29. Stewart JR, Fajardo LF, Gillette SM, Constine LS. Radiation injury to the heart. Int J Radiat Oncol Biol Phys. 1995;31(5):1205-11.

30. Kiscsatari L, Sarkozy M, Kovari B, Varga Z, Gomori K, Morvay N, et al. High-dose Radiation Induced Heart Damage in a Rat Model. In Vivo. 2016;30(5):623-31.

31. Bode F, Blanck O, Gebhard M, Hunold P, Grossherr M, Brandt S, et al. Pulmonary vein isolation by radiosurgery: implications for non-invasive treatment of atrial fibrillation. Europace. 2015;17(12):1868-74.

32. Blanck O, Bode F, Gebhard M, Hunold P, Brandt S, Bruder R, et al. Dose-escalation study for cardiac radiosurgery in a porcine model. Int J Radiat Oncol Biol Phys. 2014;89(3):590-8.

33. Sharma A, Wong D, Weidlich G, Fogarty T, Jack A, Sumanaweera T, et al. Noninvasive stereotactic radiosurgery (CyberHeart) for creation of ablation lesions in the atrium. Heart Rhythm. 2010;7(6):802-10.

34. Refaat MM, Ballout JA, Zakka P, Hotait M, Al Feghali KA, Gheida IA, et al. Swine Atrioventricular Node Ablation Using Stereotactic Radiosurgery: Methods and In Vivo Feasibility Investigation for Catheter-Free Ablation of Cardiac Arrhythmias. J Am Heart Assoc. 2017;6(11).

35. Zei PC, Wong D, Gardner E, Fogarty T, Maguire P. Safety and efficacy of stereotactic radioablation targeting pulmonary vein tissues in an

experimental model. Heart Rhythm. 2018;15(9):1420-7.

36. Straub JM, New J, Hamilton CD, Lominska C, Shnayder Y, Thomas SM. Radiation-induced fibrosis: mechanisms and implications for therapy. J Cancer Res Clin Oncol. 2015;141(11):1985-94.

37. Loo BW, Jr., Soltys SG, Wang L, Lo A, Fahimian BP, Iagaru A, et al. Stereotactic ablative radiotherapy for the treatment of refractory cardiac ventricular arrhythmia. Circ Arrhythm Electrophysiol. 2015;8(3):748-50.

38. Nath S, Lynch C, 3rd, Whayne JG, Haines DE. Cellular electrophysiological effects of hyperthermia on isolated guinea pig papillary muscle. Implications for catheter ablation. Circulation. 1993;88(4 Pt 1):1826-31.

39. Nath S, DiMarco JP, Haines DE. Basic aspects of radiofrequency catheter ablation. J Cardiovasc Electrophysiol. 1994;5(10):863-76.

40. Mazur P. Cryobiology: the freezing of biological systems. Science. 1970;168(3934):939-49.

41. Robinson CG, Samson PP, Moore KMS, Hugo GD, Knutson N, Mutic S, et al. Phase I/II Trial of Electrophysiology-Guided Noninvasive Cardiac Radioablation for Ventricular Tachycardia. Circulation. 2019;139(3):313-21.

42. Kleber AG, Saffitz JE. Role of the intercalated disc in cardiac propagation and arrhythmogenesis. Front Physiol. 2014;5:404.

43. Kontaridis MI, Geladari EV, Geladari CV. Structural Alterations in the Hypertensive Heart Disease Result in Intercalated Disc Remodeling and Arrhythmias. Hypertension and Cardiovascular Disease: Springer;

2016. p. 97-120.

44. Rizzo S, Lodder EM, Verkerk AO, Wolswinkel R, Beekman L, Pilichou K, et al. Intercalated disc abnormalities, reduced Na(+) current density, and conduction slowing in desmoglein-2 mutant mice prior to cardiomyopathic changes. Cardiovasc Res. 2012;95(4):409-18.

45. Heidenreich PA, Kapoor JR. Radiation induced heart disease: systemic disorders in heart disease. Heart. 2009;95(3):252-8.

46. Viczenczova C, Kura B, Egan Benova T, Yin C, Kukreja RC, Slezak J, et al. Irradiation-Induced Cardiac Connexin-43 and miR-21 Responses Are Hampered by Treatment with Atorvastatin and Aspirin. Int J Mol Sci. 2018;19(4).

47. Viczenczova C, Kura B, Chaudagar KK, Szeiffova Bacova B, Egan Benova T, Barancik M, et al. Myocardial connexin-43 is upregulated in response to acute cardiac injury in rats. Can J Physiol Pharmacol. 2017;95(8):911-9.

48. Viczenczova C, Szeiffova Bacova B, Egan Benova T, Kura B, Yin C, Weismann P, et al. Myocardial connexin-43 and PKC signalling are involved in adaptation of the heart to irradiation-induced injury: Implication of miR-1 and miR-21. Gen Physiol Biophys. 2016;35(2):215-22.

49. Livingston K, Schlaak RA, Puckett LL, Bergom C. The Role of Mitochondrial Dysfunction in Radiation-Induced Heart Disease: From Bench to Bedside. Front Cardiovasc Med. 2020;7:20.

50. Kam WW, Banati RB. Effects of ionizing radiation on mitochondria.

Free Radic Biol Med. 2013;65:607-19.

51. Wang H, Wei J, Zheng Q, Meng L, Xin Y, Yin X, et al. Radiation-induced heart disease: a review of classification, mechanism and prevention. Int J Biol Sci. 2019;15(10):2128-38.

52. Testani JM, Kolansky DM, Litt H, Gerstenfeld EP. Focal myocarditis mimicking acute ST-elevation myocardial infarction: diagnosis using cardiac magnetic resonance imaging. Tex Heart Inst J. 2006;33(2):256-9.

53. Qu Z, Weiss JN. Mechanisms of ventricular arrhythmias: from molecular fluctuations to electrical turbulence. Annu Rev Physiol. 2015;77:29-55.

54. Cha M, Seo K, Kim HJ, Kim M, Yoon H, Jo SW et al. Early Changes in Rat Heart After High-Dose Irradiation: Implications for Antiarrhythmic Effects of Cardiac Radioablation. J Am Heart Assoc. 2021;10:e019072.

국문 초록

치명적인 심장 부정맥인 심실 빈맥 치료에 심장 방사선 치료가 활용될 가능성을 보이는 연구 결과가 나오면서, 고에너지 방사선이 심장 근육의 전기 전도에 미치는 영향에 관심이 모아지고 있다. 암환자 치료를 위해 방사선이 활용되는 경우에 방사선이 심장에 미치는 구조적 기능적 손상에 대한 연구가 있었지만 전기 전도에 미치는 영향에 대해서는 연구가 부족하다. 심실 전도에 변화를 일으키는 기전에 대한 연구도 심근 섬유화와 심근세포 괴사가 원인이라고 추정될 뿐 심근 전도와 관련한 형태학적 변화는 아직 알려진 바가 없는데, 특히 심실 빈맥 치료의 초기 반응에 대한 연구는 전무한 실정이다. 환자 치료 경험을 기술한 이전 문헌들에 따르면 항부정맥 효과가 나타나는 시점은 환자마다 다양하여 심장 방사선 치료 후 즉시 반응이 있는 경우로부터 6개월 이후까지 보고되고 있다. 이에 본 논문에서는 연구진이 수행한 심장 방사선 치료 사례를 고찰하여 심실 빈맥 방사선 치료의 초기 반응을 조사하였으며, 고에너지 방사선을 심장에 조사하였을 때 나타나는 현상을 쥐를 이용한 실험을 통해 확인하여 심장 방사선 치료의 기전을 탐구하고자 하였다.

심장 방사선 치료 임상 시험을 수행한 5명의 환자의 방사선 치료 초기 반응을 관찰하였을 때, 모든 환자에서 2주 이내에 심실 빈맥의 정도가 감소하는 반응이 확인되었다. 또한 심실 빈맥의 빠르기가 변하고, QRS파의 형태가 변하는 것을 확인할 수 있었다.

방사선 치료 이후 심장 조직의 병리학적 변화는 쥐(rat)모델을 통하여 탐구하였다. 쥐의 심장에 고에너지 방사선을 조사하여 시간-용량-반응성 조직학적, 미세구조적, 기능적 변화를 관찰하였다. Wild type Lewis rat 95마리에서, 20, 25, 30, 40, 50 Gy의 방사선을 조사하여 1 day, 1~4 weeks에 심장을 획득하여 광학현미경 및 전자현미경으로 관찰하였다. 또한 심전도 및

심장초음파 검사를 시행하여 전기 전도와 심근 수축 능력을 평가하였다. 그 결과, 고에너지 방사선 조사에도 불구하고 심근 조직의 괴사나 사멸은 관찰되지 않았다. 하지만 사이 원반(intercalated disc)은 벌어지고 뒤틀렸으며 불규칙한 형태로 변하였다. 방사선 조사 3주차에 광범위한 세포 사이 및 세포내 부종을 관찰할 수 있었다. 또한 CD68 염색이 세포의 공포화(vacuolization)에 동반되었다. 이러한 변화는 심장의 전기 전도시스템을 구성하는 세포보다는 일반 심근세포에서 두드러졌다. 심전도의 PR 간격 및 QT 간격은 지연되었으며 ST 분절은 1주째 하강했다가, 2주차 이후에는 상승하는 결과를 보였다.

본 연구의 결론은 다음과 같다. 심실 빈맥 치료를 위한 방사선 치료의 단기 효과는 심근 섬유화나 심근 세포 괴사에 의한 것이 아니라 심근 세포의 미세구조 변화를 일으키기 때문이다. 이는 방사선 치료가 유전자의 변형을 통하여 세포괴사와 증식 억제를 일으킨다는, 종양에 대한 방사선 치료 효과와는 다른 기전이 작용하고 있음을 시사하는 소견이다. 즉 고에너지 방사선은 세포 괴사 없이 전기 전도와 세포막 전위에 영향을 주는 효과를 발생시키는 것으로 추정할 수 있었다.

주요어: 심장 방사선치료, 심실빈맥, 고주파 절제, 방사선치료, 심장근육, 초미세구조
학번: 2013-30602